# NATIONAL ADVISORY COMMITTEE FOR AERONAUTICS

**TECHNICAL NOTE 4395**

# USE OF THE KERNEL FUNCTION IN A THREE-DIMENSIONAL FLUTTER ANALYSIS WITH APPLICATION TO A FLUTTER-TESTED DELTA-WING MODEL

By Donald S. Woolston and John L. Sewall

Langley Aeronautical Laboratory
Langley Field, Va.


Washington

September 1958

NATIONAL ADVISORY COMMITTEE FOR AERONAUTICS

TECHNICAL NOTE 4395

# USE OF THE KERNEL FUNCTION IN A THREE-DIMENSIONAL FLUTTER ANALYSIS WITH APPLICATION TO A FLUTTER-TESTED DELTA-WING MODEL

By Donald S. Woolston and John L. Sewall

## SUMMARY

The development and the numerical application are presented of a Rayleigh-Ritz, or modal, type of flutter analysis which takes into account three-dimensional structural and aerodynamic behavior. The flutter mode is approximated by a series of natural-vibration modes, and the aerodynamic forces corresponding to these modes are derived from subsonic lifting-surface theory, according to the kernel-function approach, for a finite wing oscillating in compressible flow.

The application is made to a delta semispan wing with a leading-edge sweep angle of 45° which fluttered at a Mach number of 0.85. Results of flutter calculations show that, for this case, when the first three or four natural-vibration modes are used to approximate the flutter mode, converged solutions for the flutter speed are obtained that are about 5 percent less than the experimental value. Theoretical flutter-speed boundaries were located for a range of densities and Mach numbers including those of the experimental-flutter condition. Further application of the analysis to study the effects of variation in certain structural properties showed that the converged flutter speeds were more sensitive to variations in the natural frequencies than to either variations in mass or to the inclusion of generalized-mass coupling terms whose existence is due to the use of experimental natural mode shapes.

## INTRODUCTION

Current aircraft-design trends, such as the use of thinner structures and external stores on aircraft capable of very high speeds, have combined to diminish flutter safety margins and have, consequently, increased the need for greater accuracy in flutter prediction. As a result, both the structural and the aerodynamic aspects of the flutter problem should be treated by use of more realistic methods than by the beam-theory and strip-theory methods commonly employed in the past.

This report illustrates the development and application of a method of flutter analysis which takes into account three-dimensional structural and aerodynamic behavior. In treating the structural problem, the flutter mode may be approximated by a series of either natural or assumed vibration modes which could have platelike distortions or shapes. In treating the aerodynamic problem, lifting-surface theory is used to obtain aerodynamic forces which take into account finite span and compressibility as well as the modes of vibration of the structure.

In order to illustrate the application of the method, a number of flutter calculations are performed. Primary attention is directed toward correlation of the calculated result with an experimental flutter result for a delta semispan wing with a leading-edge sweep angle of $45^{\circ}$ at a Mach number of 0.85. The calculations are based on carefully measured natural-vibration modes obtained by means of an optical method. A detailed description of the determination of these modes and of the mass distribution is given in appendix A.

Other calculated results are presented for the same wing plan form in order to show some effects of variations in air density and in Mach number (for a Mach number range from 0 to 0.95). Related questions concerning the number of modes required for convergence and certain effects of nonorthogonality of the measured modes are considered. Numerical evaluation of the elements of the flutter determinant is discussed in appendix B.

## SYMBOLS

| | |
|---|---|
| $A_{ij}$ | generalized aerodynamic force (see eq. (8)) |
| $a_{nm}^{(j)}$ | arbitrary constant in series form of pressure distribution (see eq. (17)) |
| $b$ | local wing semichord, ft |
| $b_0$ | wing root semichord, ft |
| $d$ | distance between mirrors on wing surface and screen for optical method of measuring modes, in. |
| $F_n(\theta)$ | function based on chordwise pressure term (see eq. (B2)) |
| $f$ | circular frequency, cps |

| | |
|---|---|
| $\bar{f}_c, \bar{f}_s$ | constants used in numerical integration (see table VI) |
| $f_{nm}$ | dimensionless pressure mode (see eqs. (17) and (18)) |
| $g$ | structural damping coefficient |
| $h(x,y,t)$ | instantaneous deflection of point on wing surface in the flutter mode, ft |
| $h_i$ | normalized displacement at point x,y in ith mode of vibration, $h_i(x,y)$ |
| $I_c$ | chordwise integrating factor appropriate to station c (see eq. (B5)) |
| $I_s$ | spanwise integrating factor appropriate to station s (see eq. (B6)) |
| $I_{nm}^{(i)}$ | surface integral in generalized aerodynamic force (see eq. (B2)) |
| $K\left(M,\frac{\omega}{V},x-\xi,y-\eta\right)$ | kernel function of three-dimensional integral equation (see eq. (12)), 1/sq ft |
| $\bar{K}(M,k_0,\bar{x}-\bar{\xi},\bar{y}-\bar{\eta})$ | dimensionless form of three-dimensional kernel function (see eq. (14)) |
| $k_0$ | reduced-frequency parameter, $b_0\omega/V$ |
| $L_j$ | dimensionless pressure function (see eq. (5)) |
| $l$ | wing semispan, ft |
| $M$ | Mach number |
| $M_i$ | generalized mass associated with ith mode of vibration (see eq. (3)), slugs |
| $M_{ij}$ | generalized-mass coupling term (see eq. (21)), slugs |
| $m(x,y)$ | local mass per unit area at point x,y, slugs/sq ft |
| $N$ | number of sheets of aluminum foil on top or bottom surface of wing |

| | |
|---|---|
| $\Delta p(x,y,t)$ | local oscillating pressure difference between top and bottom surfaces of wing in the flutter mode (see eq. (4)), lb/sq ft |
| $\Delta p_j$ | pressure difference at point x,y in jth mode of oscillation, $\Delta p_j(x,y)$ |
| $q_i$ | generalized coordinate in ith mode of oscillation, $\bar{q}_i e^{i\omega t}$, ft |
| $\bar{q}_i$ | complex amplitude of generalized coordinate in ith mode, ft |
| S | area of wing surface, sq ft |
| t | time, sec |
| $t_I, t_F, t_B$ | thicknesses of aluminum insert, aluminum foil, and balsa, respectively (see eq. (A1)) |
| V | velocity of airstream, fps |
| $w_w$ | weight of wing per unit area, lb/sq in. |
| $x,y,\xi,\eta$ | Cartesian coordinates (see sketch following eq. (12)) |
| $\bar{x},\bar{\xi}$ | dimensionless chordwise variables referred to $b_0$ (see eq. (14)) |
| $\bar{y},\bar{\eta}$ | dimensionless spanwise variables referred to $l$ (see eq. (14)) |
| $\bar{z}$ | airfoil ordinate (see eqs. (A2) and (A3)) |
| $\alpha$ | local slope of wing in pitch during vibration, $\partial h/\partial x$ |
| $\alpha'$ | local slope of wing in a direction normal to line (or ray) of constant percent chord |
| $\bar{\alpha},\bar{\alpha}'$ | vectors representing angular displacements $\alpha$ and $\alpha'$, respectively, according to the right-hand vector rule (see eqs. (A5) and (A6) and fig. 7) |
| $\gamma_A, \gamma_B$ | unit weights of aluminum alloy and laminated balsa, respectively (see eq. (A1)), lb/cu in. |
| $\delta$ | reflected displacement on screen in optical method for measuring mode shapes, in. |

| | |
|---|---|
| $\delta_x, \delta_y$ | streamwise and spanwise components, respectively, of $\delta$ |
| $\theta$ | angular chordwise variable (see eq. (19)), deg |
| $\Lambda_r$ | angle of sweepback for rth ray, deg |
| $\mu_i$ | generalized mass-density ratio in ith mode of vibration (see eq. (10)) |
| $\rho$ | air density, slugs/cu ft |
| $\phi$ | local slope of wing in roll during vibration, $\partial h/\partial y$ |
| $\phi'$ | local slope of wing in a direction parallel to line (or ray) of constant percent chord |
| $\bar{\phi}, \bar{\phi}'$ | vectors representing angular displacements $\phi$ and $\phi'$, respectively, according to the right-hand vector rule |
| $\psi$ | angle of image, referred to the horizontal, on screen in optical method for measuring mode shapes, deg |
| $\Omega$ | complex eigenvalue of determinantal flutter equation, $\left(\frac{\omega_i}{\omega}\right)^2(1 + ig)$ |
| $\omega$ | angular frequency, $2\pi f$, radians/sec |

Indices:

| | |
|---|---|
| c,s | chordwise and spanwise stations, respectively |
| f | flutter |
| i,j | modes of vibration under consideration |
| n,m | chordwise and spanwise pressure modes, respectively, in aerodynamic quantities (m denotes power to which spanwise variable is raised; see eq. (18)) |
| r | line (or ray) of constant percent chord on wing |
| x | streamwise direction (related to local pitching direction) |
| y | spanwise direction (related to local rolling direction) |

Matrix notations:

| | |
|---|---|
| $[\ ]$ | rectangular matrix |
| $\lfloor\ \rfloor$ | row matrix |
| $\left\{\ \right\}$ | column matrix |
| $\left[\ \right]$ | diagonal matrix |

Dots over symbols denote differentiation with respect to time.

## METHOD OF FLUTTER ANALYSIS

The present section is concerned with the development of a working form of the flutter equations of a Rayleigh-Ritz, or modal, type of analysis based on aerodynamic forces obtained by subsonic lifting-surface theory. A brief discussion of the method of obtaining the aerodynamic forces is included.

### Development of Flutter Equations

In the development of the flutter equations, a basic assumption of the Rayleigh-Ritz approach is that the displacement $h(x,y,t)$ corresponding to the flutter mode may be represented by a superposition of either natural or assumed modal functions in the form

$$h(x,y,t) = q_1 h_1 + q_2 h_2 + \cdots \tag{1}$$

where $q_i = \overline{q}_i e^{i\omega t}$ is the generalized coordinate of the ith chosen mode and $h_i = h_i(x,y)$ is the corresponding normalized mode shape.

In the present investigation the normalized modal functions $h_i$ are chosen as the natural (orthogonal) modes of vibration of the structure under consideration. With this choice of mode shapes, the general equation of motion (obtained, for example, as in ref. 1) in the ith degree of freedom may be written in the form

$$M_i \ddot{q}_i + \omega_i^2 M_i q_i = \iint_S h_i \, \Delta p(x,y,t) \, dS \tag{2}$$

where $M_i$ represents the generalized mass in the ith mode and is defined as

$$M_i = \iint_S m(x,y)\, h_i^2 dS \tag{3}$$

The integral on the right side of equation (2) represents the generalized aerodynamic force and contains the aerodynamic loading $\Delta p(x,y,t)$ which, consistent with equation (1), is regarded as a superposition of aerodynamic-loading modes

$$\Delta p(x,y,t) = q_1 \Delta p_1(x,y) + q_2 \Delta p_2(x,y) + \ldots \tag{4}$$

where $\Delta p_j(x,y)$ denotes the aerodynamic loading associated with the mode shape $h_j$. In application, with $q_i = \bar{q}_i e^{i\omega t}$, $\Delta p(x,y,t)$ is expressed in terms of dimensionless functions $L_j$ through the relation

$$\Delta p(x,y,t) = 4\pi\rho V^2 \frac{l}{b_0}\left(\frac{\bar{q}_1}{b_0} L_1 + \frac{\bar{q}_2}{b_0} L_2 + \ldots\right) e^{i\omega t} \tag{5}$$

The form of the complex functions $L_j$ is dealt with at a later stage. At this stage, use may be made of equations (1) and (5) to obtain equation (2) in the form

$$\left[1 - \left(\frac{\omega_i}{\omega}\right)^2\right] M_i \bar{q}_i + \frac{4\pi\rho V^2 l}{b_0^2 \omega^2} \iint_S h_i(\bar{q}_1 L_1 + \bar{q}_2 L_2 + \ldots) dS = 0 \tag{6}$$

or, alternatively,

$$\left[1 - \left(\frac{\omega_i}{\omega}\right)^2\right] \bar{q}_i + \frac{4\pi\rho l^2 b_0}{M_i k_0^2}(\bar{q}_1 A_{i1} + \bar{q}_2 A_{i2} + \ldots) = 0 \tag{7}$$

where

$$A_{ij} = \frac{1}{b_0 l} \iint_S h_i L_j \, dS \tag{8}$$

and

$$k_0 = \frac{b_0 \omega}{V}$$

If equation (7) is written for each of the degrees of freedom under consideration, a set of simultaneous homogeneous equations results. The flutter condition is then given by the vanishing of the determinant of the coefficients of $\bar{q}_i$ in these equations; thus,

$$\begin{vmatrix} 1 - \left(\frac{\omega_1}{\omega_i}\right)^2 \Omega + \frac{A_{11}}{k_0^2 \mu_1} & \frac{A_{12}}{k_0^2 \mu_1} & \cdots \\ \frac{A_{21}}{k_0^2 \mu_2} & 1 - \left(\frac{\omega_2}{\omega_i}\right)^2 \Omega + \frac{A_{22}}{k_0^2 \mu_2} & \cdots \\ \vdots & \vdots & \vdots \end{vmatrix} = 0 \tag{9}$$

where

$$\frac{1}{\mu_i} = \frac{4\pi \rho l^2 b_0}{M_i} \tag{10}$$

and where $\Omega$ is defined by

$$\Omega = \left(\frac{\omega_i}{\omega}\right)^2 (1 + ig) \tag{11}$$

In this form $\Omega$ is a complex eigenvalue and contains the unknown frequency $\omega$ and a damping coefficient $g$ that becomes zero at the borderline flutter condition between damped and undamped motion.

Equation (9), together with the definitions given in equations (3), (8), (10), and (11), constitutes the working form of the flutter equation. In other sections of the report the determination of the ingredients of equation (9) is discussed; appendix A is concerned with the determination of mode shapes and mass distribution for a particular configuration, and appendix B deals with numerical techniques used to evaluate generalized masses and generalized aerodynamic forces.

## Determination of Aerodynamic Loading

In the determination of the aerodynamic loading, the functions $L_j$ required in the generalized aerodynamic forces are obtained from the integral equation which relates lift and downwash distributions in subsonic lifting-surface theory. (See, for example, ref. 2.) A systematic numerical solution is employed herein which is similar to that of reference 3 but which makes use of a more exact form of the kernel function together with more refined numerical-integration procedures. The method employed has been programed for the IBM type 704 electronic data processing machine.

For the purpose of the present investigation, the integral equation may be written as

$$-\left(\frac{\partial}{\partial x}+\frac{i\omega}{V}\right)h(x,y,t)=\frac{1}{4\pi\rho V^2}\iint_S K\left(M,\frac{\omega}{V},x-\xi,y-\eta\right)\Delta p(\xi,\eta,t)\,d\xi\,d\eta \qquad (12)$$

where the coordinate-axis system is shown in the following sketch:

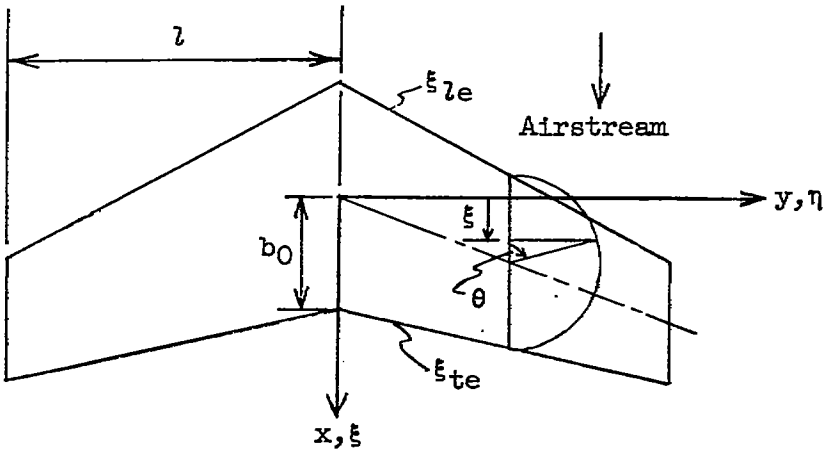

where $\xi_{le}$ and $\xi_{te}$ denote, respectively, the coordinates of the leading and trailing edges. The term on the left side of equation (12) denotes the downwash angle at point x,y associated with a displacement h(x,y,t). On the right side of equation (12), the kernel function $K\left(M,\frac{\omega}{V},x-\xi,y-\eta\right)$ represents the downwash produced at point x,y by a unit pressure load at point $\xi,\eta$; the function $\Delta p(\xi,\eta,t)$ represents the load required to satisfy the specified downwash condition. (The minus sign on the left side of eq. (12) is associated with the form of the kernel function and arises from the use herein of the sign convention for downwash, displacement, and lift which are positive downward.)

Substituting equations (1) and (5) into equation (12) gives

$$-\left(\frac{\partial}{\partial x}+\frac{i\omega}{V}\right)\left(\bar{q}_1 h_1+\bar{q}_2 h_2+\cdots\right)$$
$$=\frac{l}{b_0}\iint_S K\left(M,\frac{\omega}{V},x-\xi,y-\eta\right)\left(\frac{\bar{q}_1}{b_0}L_1+\frac{\bar{q}_2}{b_0}L_2+\cdots\right)d\xi\,d\eta \qquad (13)$$

Introducing the following dimensionless quantities

$$\left.\begin{aligned}\bar{x}&=\frac{x}{b_0}\\ \bar{\xi}&=\frac{\xi}{b_0}\\ \bar{y}&=\frac{y}{l}\\ \bar{\eta}&=\frac{\eta}{l}\\ \bar{K}(M,k_0,\bar{x}-\bar{\xi},\bar{y}-\bar{\eta})&=l^2 K\left(M,\frac{\omega}{V},x-\xi,y-\eta\right)\end{aligned}\right\} \qquad (14)$$

into equation (13) gives

$$-\left(\frac{\partial}{\partial \bar{x}} + ik_0\right)\left(\frac{\bar{q}_1}{b_0} h_1 + \frac{\bar{q}_2}{b_0} h_2 + \cdots\right)$$

$$= \iint_S \bar{K}(M,k_0,\bar{x}-\bar{\xi},\bar{y}-\bar{\eta}) \left(\frac{\bar{q}_1}{b_0} L_1 + \frac{\bar{q}_2}{b_0} L_2 + \cdots\right) d\bar{\xi}\, d\bar{\eta} \tag{15}$$

From equation (15) the form of the integral equation for the jth mode of oscillation may be seen to be

$$-\left(\frac{\partial}{\partial \bar{x}} + ik_0\right) h_j = \iint_S \bar{K}(M,k_0,\bar{x}-\bar{\xi},\bar{y}-\bar{\eta})\, L_j\, d\bar{\xi}\, d\bar{\eta} \tag{16}$$

In the solution of equation (16), it is assumed that a function $L_j$ may be represented by a series of pressure modes of the form

$$L_j = \sum_n \sum_m a_{nm}^{(j)} f_{nm} \tag{17}$$

where the quantities $a_{nm}^{(j)}$ are arbitrary constants to be determined. The indices $n$ and $m$ are associated with chordwise and spanwise pressure modes, respectively. The form of the functions $f_{nm}$ is dictated by known leading- and trailing-edge conditions. In subsonic flow they should satisfy the edge conditions pertinent to the Kutta condition. In the existing procedure for solving the integral equation they have been expressed (in terms of an angular chordwise variable $\theta$) as

$$\left.\begin{aligned} f_{0m} &= \bar{\eta}^m \sqrt{1-\bar{\eta}^2}\, \frac{b_0}{b} \cot\frac{\theta}{2} \\ f_{1m} &= \bar{\eta}^m \sqrt{1-\bar{\eta}^2}\, \frac{b_0}{b} \sin\theta \\ f_{2m} &= \bar{\eta}^m \sqrt{1-\bar{\eta}^2}\, \frac{b_0}{b} \frac{\sin 2\theta}{4} \end{aligned}\right\} \tag{18}$$

where, for example, for symmetric motion the index $m$ is equal to 0, 2, 4, . . . and where the variable $\theta$ (see sketch which follows eq. (12)) is related to $\bar{\xi}$ by the expression

$$\bar{\xi} = \frac{\bar{\xi}_{te} + \bar{\xi}_{le}}{2} - \frac{b}{b_0} \cos \theta \tag{19}$$

in which $\frac{\bar{\xi}_{te} + \bar{\xi}_{le}}{2}$ denotes the equation of the wing midchord.

If the series form of $L_j$ given by equation (17) is substituted into equation (16), a working form of the integral equation is obtained as

$$-\left(\frac{\partial}{\partial \bar{x}} + ik_0\right) h_j = \sum_n \sum_m a_{nm}^{(j)} \iint_S f_{nm} \bar{K}(M,k_0,\bar{x}-\bar{\xi},\bar{y}-\bar{\eta}) \, d\bar{\xi} \, d\bar{\eta} \tag{20}$$

and may be seen to consist of a summation of definite surface integrals, each weighted by an unknown constant $a_{nm}^{(j)}$.

In order to determine the constants $a_{nm}$, a collocation procedure is used. The right side of equation (20) is evaluated for as many points x,y, designated as control points, as there are unknown constants $a_{nm}$ and is equated to the known downwash angle at each control point. A set of simultaneous equations is thus obtained which may be solved for the values of $a_{nm}$. Once determined, the constants $a_{nm}$ are used with equations (17) and (18) to define the pressure function $L_j$; and $L_j$ may then be employed in equation (8) to obtain the generalized aerodynamic forces $A_{ij}$. In the present application nine terms of the series in equation (17) were used (so that $n = 0, 1, 2$ and $m = 0, 2, 4$), and the downwash was satisfied at the nine control points shown in figure 1(a). As previously noted, a solution of the integral equation as represented by equation (20) has recently been programed for the IBM type 704 electronic data processing machine.

## APPLICATION OF METHOD TO A DELTA WING

In order to show the application of the analytical treatment described in the preceding section, a number of calculations have been made for a

delta semispan wing with a leading-edge sweep angle of 45°. Primary attention is directed toward a correlation of calculated results with an experimental-flutter result. Other calculations are performed for the configuration of the experiment to explore some effects of varying Mach number and air density. In addition, some effects of varying mass and natural frequencies and certain effects of nonorthogonality of the measured modes are examined.

## Correlation of Calculations With Experiment

The experimental result used as a basis for the calculations has been obtained by William T. Lauten, Jr., and Marvin F. Burgess at the Langley Aeronautical Laboratory. Construction details of the 45° delta semispan wing under consideration are shown in figure 2. The mass properties of the model are shown as chordwise and spanwise distributions of weight per unit area in figure 3. The mode shapes in the first four natural modes of vibration were obtained by means of an optical method and are shown in figure 4. Details of the methods used in obtaining mass and mode shapes are described in appendix A.

Two models were involved in the experimental program. One, designated as model A, fluttered to destruction before its mode shapes and mass distribution had been determined. These structural properties were obtained by use of a second model, model B, which was built to the same specifications and had very similar nodal patterns. As can be seen in table I, model B was lighter than model A and had different natural frequencies. In all flutter calculations the mode shapes for model B were used, and in the calculations for model A the generalized masses were adjusted by the ratio of the total masses of the models.

The flutter calculation of primary interest has been made for model A, which fluttered as a cantilever at a Mach number of 0.85 with an air density of 0.000787 slugs/cu ft. Results of this flutter calculation are shown in table II(a). Converged flutter-speed solutions are obtained (as indicated by the agreement of the first three- or four-mode calculations) which are about 5 percent less than the experimental value. Calculated results based on two two-mode subcases are included in table II(a). The flutter speed calculated with modes 1 and 3 is about 2 percent above the experimental flutter speed. It is noted that modes 1 and 3 resemble, respectively, first-bending and first-torsion modes of a beam.

## Variations in Mach Number and Air Density

Results of converged flutter calculations at other values of Mach number and air density for the configuration of the experimental flutter

condition are given in table II(b) and are presented, in different forms, in figures 5 and 6. Figure 5 illustrates the effect on $V_f$ of varying density, with Mach number held constant at 0.85. Results are shown in terms of an air-density parameter $1/\sqrt{\rho}$. The effect of Mach number on calculated flutter speed is shown in figure 6 for each of three values of air density $\rho$. Results are presented in terms of a flutter-speed coefficient $V_f/b_0\omega_\beta$. As can be seen, the flutter speeds calculated for the present configuration appear to remain nearly constant for all Mach numbers up to $M = 0.95$. The corresponding calculated flutter frequencies, on the other hand, tend to decrease with increasing Mach number, as may be seen in table II(b).

## Effects of Certain Structural Modifications

The effects of the differences in total mass and natural frequencies between models A and B, noted in table I, were considered worthy of further study. First, flutter calculations were performed for model B, and the converged flutter speed was 10 percent less than that for model A. (Compare case 1 of table II(c) with the four-mode result in table II(a).) In an effort to separate the effect of the difference in total mass from the effect of the difference in natural frequencies, additional flutter calculations based on the generalized masses of model B and the natural frequencies of model A were performed. The results, listed in table II(c) (case 2), show that about three-fourths of this 10-percent difference in flutter speed was due to the differences in the natural frequencies between the two models. The remaining difference in flutter speed is then attributed to the difference in total mass.

As can be seen in equation (9), the offdiagonal elements of the flutter determinant contain no inertial-coupling terms. This is a consequence of the orthogonality condition for natural coupled modes, which may be expressed as

$$M_{ij} = \iint_S m(x,y)\, h_i h_j \, dS = 0 \qquad (i \neq j) \qquad (21)$$

It is recalled that, in the present analysis, measured modes were employed. In order to investigate their orthogonality, values of $M_{ij}$ were computed for model A by use of equation (21) and are listed in table III. In order to determine the effects of the nonzero values of $M_{ij}$, they were added to the appropriate elements of equation (9) and two calculations were made for model A. First, the aerodynamic terms were eliminated and the natural frequencies were computed; results

are shown in table III and, with the exception of $f_4$, are seen to differ by a negligible amount from those in table I. In a second calculation the change in flutter speed due to including the $M_{ij}$ terms was determined; the other parameters used were those of the four-mode solution of table II(a). Results are listed as case 3 of table II(c) and show that the converged flutter speed has been decreased by less than 1 percent.

## CONCLUDING REMARKS

The development and the numerical application have been presented of a method of flutter analysis which takes into account three-dimensional structural and aerodynamic behavior. The flutter mode was approximated by a series of natural-vibration modes, and the aerodynamic forces corresponding to these modes were derived from subsonic lifting-surface theory, according to the kernel-function approach, for a finite wing oscillating in compressible flow.

The application was made to a delta semispan wing with a leading-edge sweep angle of 45° which fluttered at a Mach number of 0.85. Results of flutter calculations show that when the first three or four natural-vibration modes were included, converged solutions for the flutter speed were obtained which were about 5 percent less than the experimental value. Further application of the analysis was made to orient the experimental flutter condition with theoretical flutter-speed boundaries for a range of densities and Mach numbers including those of the experiment and to study the effects of certain variations in natural frequencies and total mass.

Langley Aeronautical Laboratory,
National Advisory Committee for Aeronautics,
Langley Field, Va., July 17, 1958.

# APPENDIX A

## STRUCTURAL PROPERTIES OF DELTA-WING MODEL

The structural properties of the delta-wing model needed for the flutter analysis that is presented and applied in this report consist of the mass distribution and the natural modes of vibration, which are represented in equations (3) and (8) as $m(x,y)$ and $h_i$, respectively. This appendix provides a description of the methods used to determine these properties for the delta-wing configuration considered in this analysis.

### Description of Model

Figure 2 shows pertinent details of the construction of the model. This construction consisted of a 0.02-inch-thick sheet of aluminum alloy located at the plane of symmetry with vertically laminated balsa glued to each surface of the sheet. The balsa laminations were shaped to the ordinates of an NACA 65A004 airfoil section, and the outside surface was wrapped with layers of 0.001-inch-thick aluminum foil. The wing tip was rounded so that the semispan was 32.85 inches at a point 1.5 inches forward of the trailing edge. The aerodynamic aspect ratio, with the assumption of a straight or squared-off tip based on extensions of leading and trailing edges to a common point, was 3.54.

Two models were involved, both built to the same specifications. One model, designated as model A, fluttered to destruction before all of its properties were determined; the other model, model B, was used to obtain the mass distribution and experimental natural-mode shapes for these elements. Certain mechanical properties of both models are compared in table I.

### Mass Properties of Model

The mass properties of both models studied in this investigation are based on the chordwise and spanwise distributions of weight per unit area shown in figure 3. These distributions were calculated from the equation

$$w_w = \gamma_A \left(t_I + t_F\right) + \gamma_B t_B \qquad (A1)$$

where $w_w$ is the weight of the wing per unit area, $\gamma_A$ is the unit weight of aluminum alloy, $t_I$ is the thickness of the aluminum insert,

$t_F$ is the thickness of the aluminum foil, $t_B$ is the thickness of the laminated balsa, and $\gamma_B$ is the unit weight of laminated balsa. The value of $\gamma_B$, which was determined from the measured total weight of the wing and the volume occupied by the balsa, was found to be 0.01007 lb/cu in. By using this value together with $\gamma_A$ = 0.100 lb/cu in. and the data given in figure 2, equation (A1) can be written in the form

$$w_w = 0.100(0.020 + 0.002N) + 0.01007\left[48\bar{z}b - (0.02 + 0.002N)\right] \qquad (A2)$$

everywhere on the wing except in the regions of the leading and trailing edges which were covered by an additional layer of aluminum foil which was $1\frac{1}{4}$ inches wide on each surface. The consequent increase in weight in these edge regions was accounted for in the equation

$$w_w = 0.100(0.022 + 0.002N) + 0.01007\left[48\bar{z}b - (0.022 + 0.002N)\right] \qquad (A3)$$

In equations (A2) and (A3) N is the number of 0.001-inch-thick sheets of aluminum foil on each (top or bottom) surface of the wing, and $\bar{z}$ is the ratio of one-half the local thickness to the local chord for an NACA 65A004 airfoil.

## Optical Method of Measuring Natural-Vibration Modes

The natural-vibration modes were obtained from the results of shake tests conducted at zero airspeed and involving the use of an electrodynamic shaker. The shaker was located near the wing root in order to reduce as much as possible the effect of the shaker mass on the natural modes. For each natural frequency found, the corresponding mode shape up through the fourth mode was determined by application of an optical method described in this section. This method involved the measurements and numerical integration of local slopes in pitch and roll directions at 24 stations distributed over the wing surface.

A schematic diagram of the apparatus used in this optical method is shown in figure 7. Small mirrors that were 1/16 inch square were glued to the wing at six stations along rays at 25, 50, and 75 percent chord and along the trailing edge as shown in the mirror lattice in the upper left corner of the figure. Light aimed at the wing was reflected by the mirrors onto a screen located a considerable distance from the model. During vibration in a natural mode, images reflected from these mirrors appeared as straight lines whose lengths and directions were marked on the screen. These measured lengths and directions were resolved into

local pitching and rolling slopes for small values of $\alpha$ and $\phi$ by the relations

$$\left.\begin{aligned} \alpha &\approx \frac{\delta_x}{2d} = \frac{\delta}{2d}\cos\psi \\ \phi &\approx \frac{\delta_y}{2d} = \frac{\delta}{2d}\sin\psi \end{aligned}\right\} \tag{A4}$$

It should be noted that, although this relation is shown for an instantaneous position of the model from equilibrium, it also applies when $\delta$ corresponds to a double amplitude, as is the case during vibration. The distance $d$ in this application was 155 inches.

The local slopes in pitch and roll were obtained at six stations along each of four rays at 25, 50, 75, and 100 percent chord. Deflections along each ray were determined by numerically integrating spanwise curves faired through the six values of $\phi'$ along the ray. The vectors $\bar{\alpha}$, $\bar{\alpha}'$, $\bar{\phi}$, and $\bar{\phi}'$ indicated in the lower left corner of figure 7 represent angular displacements $\alpha$, $\alpha'$, $\phi$, and $\phi'$, respectively, according to the right-hand vector rule, and from this vector relationship

$$\left.\begin{aligned} \alpha &= \alpha'\cos\Lambda_r + \phi'\sin\Lambda_r \\ \phi &= -\alpha'\sin\Lambda_r + \phi'\cos\Lambda_r \end{aligned}\right\} \tag{A5}$$

from which

$$\phi' = \phi\cos\Lambda_r + \alpha\sin\Lambda_r \tag{A6}$$

Thus, for the ith natural mode, after substitution of equation (A4) into equation (A6),

$$\phi' \equiv \phi'^{(i)}_{sr} = \frac{\delta^{(i)}_{sr}}{2d}\sin\left(\psi^{(i)}_{sr} + \Lambda_r\right) \qquad (i = 1,2,3,4) \tag{A7}$$

where the subscripts $s$ and $r$ identify a point on the mirror lattice as indicated in the upper left corner of figure 7. Values of $\phi'^{(i)}_{sr}$ determined from this equation are given in table IV. For modes higher than the first mode, the sign of the angle $\psi^{(i)}_{sr} + \Lambda_r$ was governed by the observed node locations on the rays rather than by the actual numerical value of this angle.

These slopes were in turn used to determine the deflections by numerically integrating spanwise curves faired through the six values of $\phi'$ along each ray. A check of the data disclosed that, for any point on a particular ray, the deflection obtained in this manner was in very close agreement with the deflection obtained by integrating $\phi'$ along the trailing edge to the spanwise position of the point and then by integrating the curve faired through four chordwise values of $\alpha_{sr}^{(i)}$ forward of the trailing edge to the point itself. On the basis of this check, the normalized deflection curves shown in figure 4 for the first four modes have been adjusted to be compatible with the measured values of $\alpha_{sr}^{(i)}$ given in table V.

The integration of $\phi'$ along a ray was performed by means of the direct-summation method illustrated in reference 4 with the use of 10 equally spaced stations for the first mode, 15 to 17 stations for the second mode, 11 to 14 stations for the third mode, and 18 and 19 stations for the fourth mode.

The nodes shown in figures 4(b), 4(c), and 4(d) trace out very nearly the same paths observed on model A, particularly in the outboard region of the wing plan form. Because this similarity is a good, though not complete, indication of mode-shape similarity between the two models, the mode shapes used to calculate the generalized masses of model A were assumed to be the same as those measured for model B.

# APPENDIX B

## EVALUATION OF ELEMENTS OF DETERMINANTAL FLUTTER EQUATION AND APPLICATION TO A SPECIFIC CONFIGURATION

### Evaluation of Generalized Aerodynamic Force

In order to evaluate the generalized aerodynamic force $A_{ij}$ (eq. (8)), use is made of the dimensionless variables introduced by equation (14) and the pressure function $L_j$ given by equations (17) to (19) to write equation (8) as

$$A_{ij} = \int_0^1 \int_0^\pi h_i \sqrt{1 - \bar{y}^2} \left[ \cot \frac{\theta}{2} \left( a_{00} + \bar{y}^2 a_{02} + \ldots \right) + \sin \theta \left( a_{10} + \bar{y}^2 a_{12} + \ldots \right) + \frac{1}{4} \sin 2\theta \left( a_{20} + \bar{y}^2 a_{22} + \ldots \right) + \ldots \right] \sin \theta \, d\theta \, d\bar{y} \qquad \text{(B1)}$$

In the evaluation of this equation, the following definitions are useful:

$$\left.\begin{aligned} F_0(\theta) &= \cot \frac{\theta}{2} \sin \theta = 1 + \cos \theta \\ F_1(\theta) &= \sin^2 \theta \\ F_2(\theta) &= \frac{1}{4} \sin 2\theta \sin \theta \\ I_{nm}^{(i)} &= \int_0^1 \int_0^\pi \bar{y}^m \sqrt{1 - \bar{y}^2} \, F_n(\theta) \, h_i \, d\theta \, d\bar{y} \end{aligned}\right\} \qquad \text{(B2)}$$

Equation (B1) may be written in terms of the integral $I_{nm}^{(i)}$ as the summation

$$A_{ij} = \sum_n \sum_m I_{nm}^{(i)} \, a_{nm}^{(j)} \qquad \text{(B3)}$$

or, as the matrix product

$$A_{ij} = \left[I_{nm}^{(i)}\right]\left\{a_{nm}^{(j)}\right\} = \left[I_{00}^{(i)} \cdots I_{nm}^{(i)} \cdots\right]\begin{Bmatrix} a_{00}^{(j)} \\ \vdots \\ a_{nm}^{(j)} \end{Bmatrix} \tag{B4}$$

Numerical integrating techniques can be applied to evaluate the surface integrals $I_{nm}$ in the row matrix of equation (B4). (It is noted in this connection that the use of the angular coordinate $\theta$ in the chordwise integration is particularly convenient for this application. For example, when represented in Cartesian coordinates, the first term in the integrand of $I_{0m}^{(i)}$ is infinite at the wing leading edge; when expressed in polar coordinates, the product $\cot\frac{\theta}{2}\sin\theta$ is a nonsingular function.) A number of spanwise stations may be chosen at $\bar{y} = \bar{y}_s$ with appropriate spanwise integrating factors $I_s$. Similarly, at each spanwise station, a number of chordwise stations are selected at $\theta = \theta_c$ with appropriate chordwise integrating factors $I_c$; s and c thus identify stations on an integrating lattice such as that shown in figure 1(b).

A matrix product of chordwise terms may be formed as

$$\underset{n\downarrow}{\overset{c\rightarrow}{[\theta]}} = \underset{n\downarrow}{\overset{c\rightarrow}{[F_n(\theta_c)]}}\left[I_c\right] = \begin{bmatrix} I_1 F_0(\theta_1) & I_2 F_0(\theta_2) & \cdots \\ I_1 F_1(\theta_1) & I_2 F_1(\theta_2) & \cdots \\ \vdots & \vdots & \vdots \\ \vdots & \vdots & \vdots \\ \vdots & \vdots & \vdots \end{bmatrix} \tag{B5}$$

and a matrix product of spanwise terms may be formed as

$$\underset{s\downarrow}{\overset{m\rightarrow}{[\bar{Y}]}} = \left[I_s\right]\underset{s\downarrow}{\overset{m\rightarrow}{\left[\bar{y}_s^{\,m}\sqrt{1-\bar{y}_s^{\,2}}\right]}} = \begin{bmatrix} I_1\sqrt{1-\bar{y}_1^{\,2}} & I_1\bar{y}_1^{\,2}\sqrt{1-\bar{y}_1^{\,2}} & \cdots \\ I_2\sqrt{1-\bar{y}_2^{\,2}} & I_2\bar{y}_2^{\,2}\sqrt{1-\bar{y}_2^{\,2}} & \cdots \\ \vdots & \vdots & \vdots \\ \vdots & \vdots & \vdots \\ \vdots & \vdots & \vdots \end{bmatrix} \tag{B6}$$

The normalized displacements $h_i$ at the integrating stations may be arranged in a rectangular matrix of the form

$$\underset{c\downarrow}{\overset{s\rightarrow}{\left[h_i\right]}} = \begin{bmatrix} h_i(\theta_1,\bar{y}_1) & h_i(\theta_1,\bar{y}_2) & \cdots & h_i(\theta_1,\bar{y}_s) \\ h_i(\theta_2,\bar{y}_1) & \cdot & \cdot & \cdot \\ \vdots & \vdots & \vdots & \vdots \\ h_i(\theta_c,\bar{y}_1) & \cdot & \cdot & \cdot \end{bmatrix} \tag{B7}$$

Equations (B5) to (B7) may be used to obtain the surface integrals $I_{nm}^{(i)}$ of equation (B2) from the matrix product

$$\underset{n\downarrow}{\overset{m\rightarrow}{\left[I_{nm}^{(i)}\right]}} = [\Theta][h_i][\bar{Y}] \tag{B8}$$

The elements of the rectangular matrix on the left side of equation (B8) may then be rearranged as the row matrix $\left[I_{nm}^{(i)}\right]$ of equation (B4) and be used with the values of the constants $a_{nm}^{(j)}$ to obtain the generalized aerodynamic force $A_{ij}$. Equation (B4) may, of course, be expanded for any number of modes into

$$\begin{bmatrix} A_{11} & A_{12} & \cdots & A_{ij} \\ A_{21} & \cdot & \cdot & \cdot \\ \vdots & \vdots & \vdots & \vdots \\ A_{i1} & \cdot & \cdot & \cdot \end{bmatrix} = \begin{bmatrix} I_{00}^{(1)} & \cdots & I_{nm}^{(1)} \\ \vdots & \vdots & \vdots \\ I_{00}^{(i)} & \cdot & \cdot \end{bmatrix} \begin{bmatrix} a_{00}^{(1)} & \cdots & a_{00}^{(j)} \\ \vdots & \vdots & \vdots \\ a_{nm}^{(1)} & \cdot & \cdot \end{bmatrix} \tag{B9}$$

## Evaluation of Generalized Mass

The generalized mass $M_i$ is expressed as a surface integral by equation (3) and may be evaluated by use of the same matrices of integrating factors and displacements employed in evaluating the generalized aerodynamic forces $A_{ij}$. For this purpose, equation (3) may be written in terms of the variables defined by equations (14) and (19) as

$$M_i = b_0 l \int_0^1 \int_0^{\pi} h_i^2 \, m\left(\theta_1, \bar{y}\right) \frac{b}{b_0} \sin\theta \, d\theta \, d\bar{y} \tag{B10}$$

or, as a summation which involves the integrating factors $I_s$ and $I_c$ used with $A_{ij}$, in the form

$$M_i = b_0 l \sum_s \sum_c I_s \frac{b_s}{b_0} I_c \, m\left(\theta_c, \bar{y}_s\right) h_i^2\left(\theta_c, \bar{y}_s\right) \sin\theta_c \tag{B11}$$

or in terms of a matrix product as

$$M_i = b_0 l \sum_s I_s \frac{b_s}{b_0} \left[ m\left(\theta_c, \bar{y}_s\right) I_c \sin\theta_c \right]^{c \rightarrow} \left\{ h_i^2\left(\theta_c, \bar{y}_s\right) \right\}^{c \downarrow} \tag{B12}$$

The column matrix $\left\{h_i^2\right\}$, which pertains to a particular spanwise station, may be obtained by squaring the elements in the corresponding column in the matrix $\left[h_i\right]$ (eq. (B7)). The inertial-coupling term $M_{ij}$ (eq. (21)) is found by replacing the matrix $\left\{h_i^2\left(\theta_c, \bar{y}_s\right)\right\}$ in equation (B12) with a matrix of crossproducts $\left\{h_i h_j\right\}$ for $i \neq j$.

## Application of Method to a Specific Configuration

In the application to a specific configuration of the integrating procedures discussed in the previous section, either equal or unequal intervals in a given variable may be taken. With equal intervals, appropriate integrating factors are readily available; when unequal intervals are employed, corresponding integrating factors must be developed. Useful procedures relating to numerical integration are presented in reference 5.

In the present application to the flutter of a delta wing, 10 equal intervals in the chordwise variable $\theta$ and 8 equal intervals in the spanwise variable $\bar{y}$ were used. The integration stations are shown in figure 1(b). Chordwise integrating factors $I_c$ employed are based on a rule employing overlapping quintic functions derived in reference 4. Spanwise integrating factors $I_s$ were based on a rule which employs overlapping quartic functions. Data pertinent to the evaluation of the factors $I_c$ and $I_s$ are given in table VI.

Normalized mode shapes $h_i$ employed in obtaining both generalized force $A_{ij}$ and generalized mass $M_i$ were obtained from the plots of figure 4. The normalizing station for each mode was arbitrarily located on the midchord at $\bar{y} = 0.875$. Values of mass per unit area $m(\theta_c, \bar{y}_s)$ for use in determining $M_i$ were obtained from the weight distribution shown in figure 3. The components $\frac{\partial h_i}{\partial \bar{x}}$ and $h_j$ of the downwash angle employed as a boundary condition in equation (20) are listed in table VII for the control points shown in figure 1(a).

## REFERENCES

1. Bisplinghoff, Raymond L., Ashley, Holt, and Halfman, Robert L.: Aeroelasticity. Addison-Wesley Pub. Co., Inc. (Cambridge, Mass.), c.1955, pp. 555-557.

2. Watkins, Charles E., Runyan, Harry L., and Woolston, Donald S.: On the Kernel Function of the Integral Equation Relating the Lift and Downwash Distributions of Oscillating Finite Wings in Subsonic Flow. NACA Rep. 1234, 1955. (Supersedes NACA TN 3131.)

3. Runyan, Harry L., and Woolston, Donald S.: Method for Calculating the Aerodynamic Loading on an Oscillating Finite Wing in Subsonic and Sonic Flow. NACA Rep. 1322, 1957. (Supersedes NACA TN 3694.)

4. Houbolt, John C., and Anderson, Roger A.: Calculation of Uncoupled Modes and Frequencies in Bending or Torsion of Nonuniform Beams. NACA TN 1522, 1948.

5. Sokolnikoff, Ivan S., and Sokolnikoff, Elizabeth S.: Higher Mathematics for Engineers and Physicists. Second ed., McGraw-Hill Book Co., Inc., 1941, pp. 550-560.

TABLE I

CERTAIN MECHANICAL PROPERTIES OF DELTA-WING MODELS

| Item | Model A | Model B |
|---|---|---|
| Aspect ratio (squared-off tip) | 3.54 | 3.54 |
| Airfoil section | NACA 65A004 | NACA 65A004 |
| $\Lambda_r$, deg: | | |
| Leading edge | 45 | 45 |
| 25 percent chord (r = 1) | 36.83 | 36.83 |
| 50 percent chord (r = 2) | 26.58 | 26.58 |
| 75 percent chord (r = 3) | 14.03 | 14.03 |
| Trailing edge (r = 4) | 0 | 0 |
| $b_0$, ft | 1.458 | 1.458 |
| $l$, ft | 2.739 | 2.739 |
| Total mass of wing, lb-sec$^2$/ft | 0.1789 | 0.1644 |
| Natural frequencies, cps: | | |
| First mode | 21 | 21 |
| Second mode | 58 | 52.5 |
| Third mode | 81 | 77 |
| Fourth mode | 115 | 107 |

TABLE II

RESULTS OF FLUTTER ANALYSIS AND CORRELATION WITH EXPERIMENT

(a) Correlation of theory and experiment for model A
(M = 0.85; $\rho$ = 0.000787 slugs/cu ft)

| | Modes used in analysis | $V_f$, fps | $f_f$, cps | $k_{0,f}$ |
|---|---|---|---|---|
| Results of calculations | 1, 2 | 2,405 | 73.5 | 0.280 |
| | 1, 3 | 943 | 41.5 | .403 |
| | 1, 2, 3 | 882 | 40.0 | .415 |
| | 1, 2, 3, 4 | 876.5 | 39.8 | .416 |
| Experiment | ---------- | 924 | 37.9 | 0.375 |

(b) Results of converged flutter calculations at other Mach numbers and densities
(Four modes used in analysis)

| M | $\rho$, slugs/cu ft | $V_f$, fps | $f_f$, cps | $k_{0,f}$ | M | $\rho$, slugs/cu ft | $V_f$, fps | $f_f$, cps | $k_{0,f}$ |
|---|---|---|---|---|---|---|---|---|---|
| 0.85 | 0.000504 | 1,094 | 39.3 | 0.329 | 0 | 0.000787 | 916 | 53.5 | 0.535 |
| | .001267 | 720 | 40.2 | .511 | .4 | | 930 | 52.1 | .513 |
| | .0021 | 618 | 42.5 | .630 | .7 | | 920 | 46.0 | .458 |
| | .00326 | 554 | 43.9 | .726 | .95 | | 928 | 38.0 | .375 |
| 0 | 0.000504 | 1,129 | 53.0 | 0.430 | 0 | 0.001267 | 735 | 54.0 | 0.673 |
| .4 | | 1,133 | 51.2 | .414 | .4 | | 741 | 52.6 | .650 |
| .7 | | 1,135 | 45.5 | .367 | .7 | | 752 | 46.8 | .570 |
| .95 | | 1,073 | 36.9 | .315 | .95 | | 792 | 42.2 | .488 |

(c) Effects of structural modifications
(M = 0.85; $\rho$ = 0.000787 slugs/cu ft)

| Case | Model | $M_{ij}$ $(i \neq j)$ | Results of converged solutions | | |
|---|---|---|---|---|---|
| | | | $V_f$, fps | $f_f$, cps | $k_{0,f}$ |
| 1 | B | 0 | 797 | 38.2 | 0.439 |
| 2 | (a) | 0 | 857 | 40.0 | .428 |
| 3 | A | Nonzero | 872 | 39.0 | .410 |

[a]The model combined the generalized masses of model B and the natural frequencies of model A.

TABLE III

GENERALIZED MASSES AND CORRESPONDING CALCULATED NATURAL FREQUENCIES COMPUTED FROM EQUATION (21) FOR MODEL A

| i | $M_{ij}$, slugs, for values of j of — | | | | $f_i$, cps |
|---|---|---|---|---|---|
| | 1 | 2 | 3 | 4 | |
| 1 | 0.010376 | -0.0015128 | 0.0034925 | -0.026760 | 20.95 |
| 2 | -.0015128 | .0159856 | -.0139947 | -.0645656 | 57.2 |
| 3 | .0034925 | -.0139947 | 1.243043 | -.0471072 | 81.6 |
| 4 | -.026760 | -.0645656 | -.0471072 | 2.897119 | 125.7 |

TABLE IV

MEASURED SLOPES $\phi'^{(i)}_{sr}$ OF NATURAL-VIBRATION MODE SHAPES

CALCULATED BY MEANS OF EQUATION (A7)[a]

| i | s | Semispan station, percent | r = 1 (25 percent chord) | r = 2 (50 percent chord) | r = 3 (75 percent chord) | r = 4 (trailing edge) |
|---|---|---|---|---|---|---|
| 1 | 1 | 20 | 0.280 | 0.727 | 1.096 | 1.350 |
| | 2 | 35 | 1.048 | 1.570 | 1.870 | 2.550 |
| | 3 | 50 | 2.298 | 2.964 | 3.410 | 4.080 |
| | 4 | 65 | 4.001 | 4.495 | 4.927 | 5.284 |
| | 5 | 80 | 5.842 | 6.373 | 6.755 | 6.794 |
| | 6 | 90 | 7.707 | 7.937 | 7.916 | 7.621 |
| 2 | 1 | 20 | -0.658 | -0.786 | -1.243 | -1.873 |
| | 2 | 35 | -1.150 | -1.208 | -1.526 | -1.777 |
| | 3 | 50 | -.993 | -.605 | -.175 | .481 |
| | 4 | 65 | .992 | 1.888 | 2.868 | 4.012 |
| | 5 | 80 | 6.029 | 7.245 | 8.683 | 10.046 |
| | 6 | 90 | 11.938 | 12.558 | 12.978 | 12.915 |
| 3 | 1 | 20 | 0.891 | 0.659 | -0.968 | -3.355 |
| | 2 | 35 | 1.037 | .065 | -1.262 | -3.117 |
| | 3 | 50 | .783 | -.205 | -1.055 | -1.207 |
| | 4 | 65 | -.1195 | -.259 | -.116 | 1.217 |
| | 5 | 80 | -.622 | .125 | 1.539 | 3.636 |
| | 6 | 90 | -.4505 | 1.012 | 2.854 | 4.987 |
| 4 | 1 | 20 | 0.436 | 0.455 | 0.667 | 1.538 |
| | 2 | 35 | .303 | .239 | .243 | -.356 |
| | 3 | 50 | -.591 | -.987 | -1.492 | -3.022 |
| | 4 | 65 | -1.830 | -1.720 | -1.877 | -2.200 |
| | 5 | 80 | .373 | 1.486 | 3.017 | 4.788 |
| | 6 | 90 | 7.963 | 9.029 | 9.196 | 8.772 |

[a]Each slope may be obtained by multiplying the corresponding value in the table by 0.003225.

TABLE V

MEASURED SLOPES IN PITCH $\alpha_{sr}^{(i)}$ OF NATURAL-VIBRATION-MODE SHAPES[a]

| i | s | Semispan station, percent | r = 1 (25 percent chord) | r = 2 (50 percent chord) | r = 3 (75 percent chord) | r = 4 (trailing edge) |
|---|---|---|---|---|---|---|
| 1 | 1 | 20 | 0.1063 | 0.204 | 0.0968 | -0.166 |
| | 2 | 35 | .572 | .540 | .484 | .0445 |
| | 3 | 50 | 1.19 | 1.16 | .854 | .610 |
| | 4 | 65 | 2.015 | 1.83 | 1.655 | 1.416 |
| | 5 | 80 | 2.735 | 2.69 | 2.62 | 2.47 |
| | 6 | 90 | 3.61 | 3.355 | 3.34 | 3.315 |
| 2 | 1 | 20 | -0.205 | -0.221 | -0.174 | -0.164 |
| | 2 | 35 | -.446 | -.2895 | -.473 | -.755 |
| | 3 | 50 | .1208 | -.0836 | -.348 | -1.13 |
| | 4 | 65 | 1.02 | .931 | .499 | -.2455 |
| | 5 | 80 | 3.54 | 3.01 | 2.98 | 2.32 |
| | 6 | 90 | 6.18 | 5.80 | 5.59 | 5.49 |
| 3 | 1 | 20 | -0.074 | -1.29 | -1.295 | -1.78 |
| | 2 | 35 | -.556 | -1.713 | -3.05 | -4.14 |
| | 3 | 50 | -2.015 | -3.495 | -5.05 | -6.50 |
| | 4 | 65 | -4.19 | -5.26 | -6.65 | -7.69 |
| | 5 | 80 | -6.26 | -6.94 | -7.70 | -8.15 |
| | 6 | 90 | -7.55 | -7.58 | -7.85 | -7.98 |
| 4 | 1 | 20 | -0.172 | 0.067 | 0.335 | 0.835 |
| | 2 | 35 | .028 | .084 | .483 | 1.426 |
| | 3 | 50 | -.474 | -.301 | .082 | .479 |
| | 4 | 65 | .791 | -.483 | -.743 | -1.270 |
| | 5 | 80 | .790 | .767 | .371 | -.461 |
| | 6 | 90 | 4.515 | 4.172 | 3.640 | 2.937 |

[a]Each slope may be obtained by multiplying the corresponding value in the table by 0.003225.

TABLE VI

DATA EMPLOYED IN NUMERICAL INTEGRATION

(a) Chordwise integration $\left(I_c = \frac{125}{144} \Delta\theta \bar{f}_c;\ \Delta\theta = \frac{\pi}{10}\right)$

| | Chordwise station, c | | | | | | | | | | |
|---|---|---|---|---|---|---|---|---|---|---|---|
| | 1 | 2 | 3 | 4 | 5 | 6 | 7 | 8 | 9 | 10 | 11 |
| $\theta_c$, deg . . . . | 0 | 18 | 36 | 54 | 72 | 90 | 108 | 126 | 144 | 162 | 180 |
| $\bar{f}_c$ . . . . . | .38 | 1.50 | 1.00 | 1.00 | 1.50 | .76 | 1.50 | 1.00 | 1.00 | 1.50 | .38 |

(b) Spanwise integration $\left(I_s = \frac{2}{45} \Delta\bar{y} \bar{\bar{f}}_s;\ \Delta\bar{y} = 0.125\right)$

| | Spanwise station, s | | | | | | | | |
|---|---|---|---|---|---|---|---|---|---|
| | 1 | 2 | 3 | 4 | 5 | 6 | 7 | 8 | 9 |
| $\bar{y}_s$ . . . . | 0 | 0.125 | 0.250 | 0.375 | 0.500 | 0.625 | 0.750 | 0.875 | 1.000 |
| $\bar{f}_s$ . . . . | 7 | 32 | 12 | 32 | 14 | 32 | 12 | 32 | 7 |
| $b_s/b_0$ . . | 1.000 | .8827 | .7654 | .6480 | .5307 | .4134 | .2961 | .1788 | .0614 |

TABLE VII

DOWNWASH BOUNDARY CONDITIONS EMPLOYED IN EQUATION (20) FOR MEASURED NATURAL-VIBRATION-MODE SHAPES

| Control point (a) | Semispan station, percent | First mode | | Second mode | | Third mode | | Fourth mode | |
|---|---|---|---|---|---|---|---|---|---|
| | | $\frac{\partial h_1}{\partial \bar{x}}$ | $h_1$ | $\frac{\partial h_2}{\partial \bar{x}}$ | $h_2$ | $\frac{\partial h_3}{\partial \bar{x}}$ | $h_3$ | $\frac{\partial h_4}{\partial \bar{x}}$ | $h_4$ |
| 1 | 20 | 0.02096 | 0.0175 | -0.1015 | -0.07015 | -0.348 | 1.500 | -3.24 | 2.50 |
| 2 | | .04025 | .0350 | -.1094 | -.1404 | -6.065 | .833 | 1.26 | 2.00 |
| 3 | | .0191 | .0594 | -.0862 | -.1666 | -6.095 | -1.084 | 6.30 | 3.67 |
| 4 | 50 | 0.235 | 0.1784 | 0.05985 | -0.4515 | -9.48 | 4.33 | -8.93 | 3.165 |
| 5 | | .229 | .2412 | -.04135 | -.4605 | -16.45 | 1.00 | -5.67 | 2.667 |
| 6 | | .1684 | .2869 | -.1722 | -.4955 | -23.79 | -4.165 | 1.54 | 1.334 |
| 7 | 80 | 0.540 | 0.731 | 1.751 | 0.1053 | -29.45 | 4.375 | 14.87 | -11.66 |
| 8 | | .5315 | .794 | 1.490 | .298 | -32.65 | .625 | 14.41 | -11.16 |
| 9 | | .517 | .8535 | 1.475 | .4649 | -36.15 | -3.75 | 6.98 | -10.0 |

[a] Control points are shown in figure 1(a).

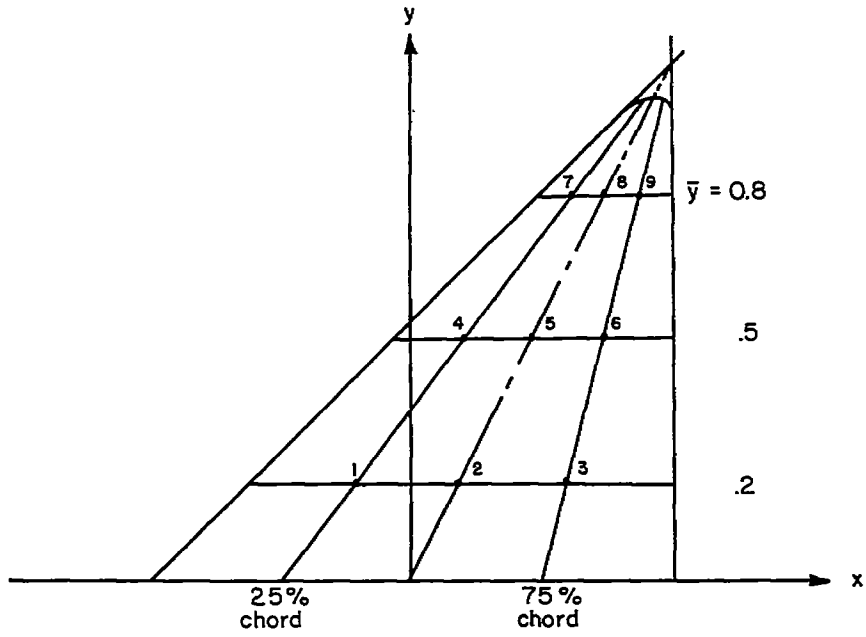


(a) Control points.

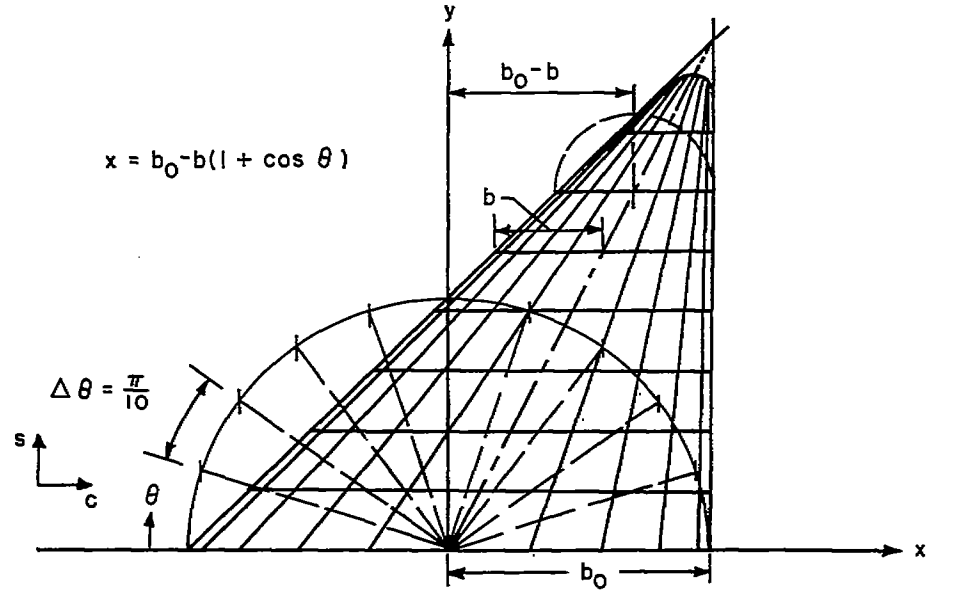


(b) Numerical integration.

Figure 1.- Lattices used in evaluation of elements of flutter determinant for 45° delta semispan wing.

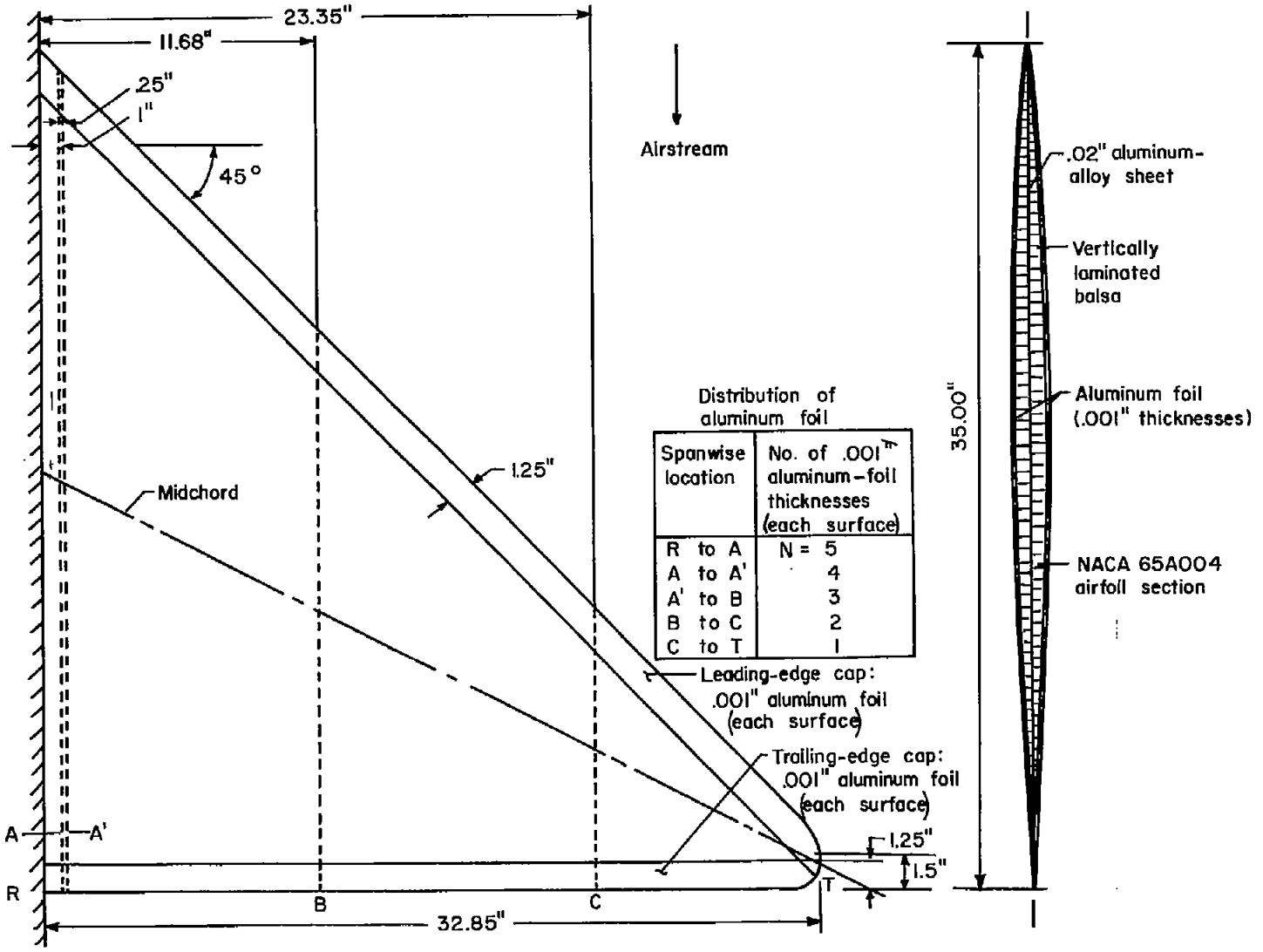


Figure 2.- Construction details of delta-wing model.

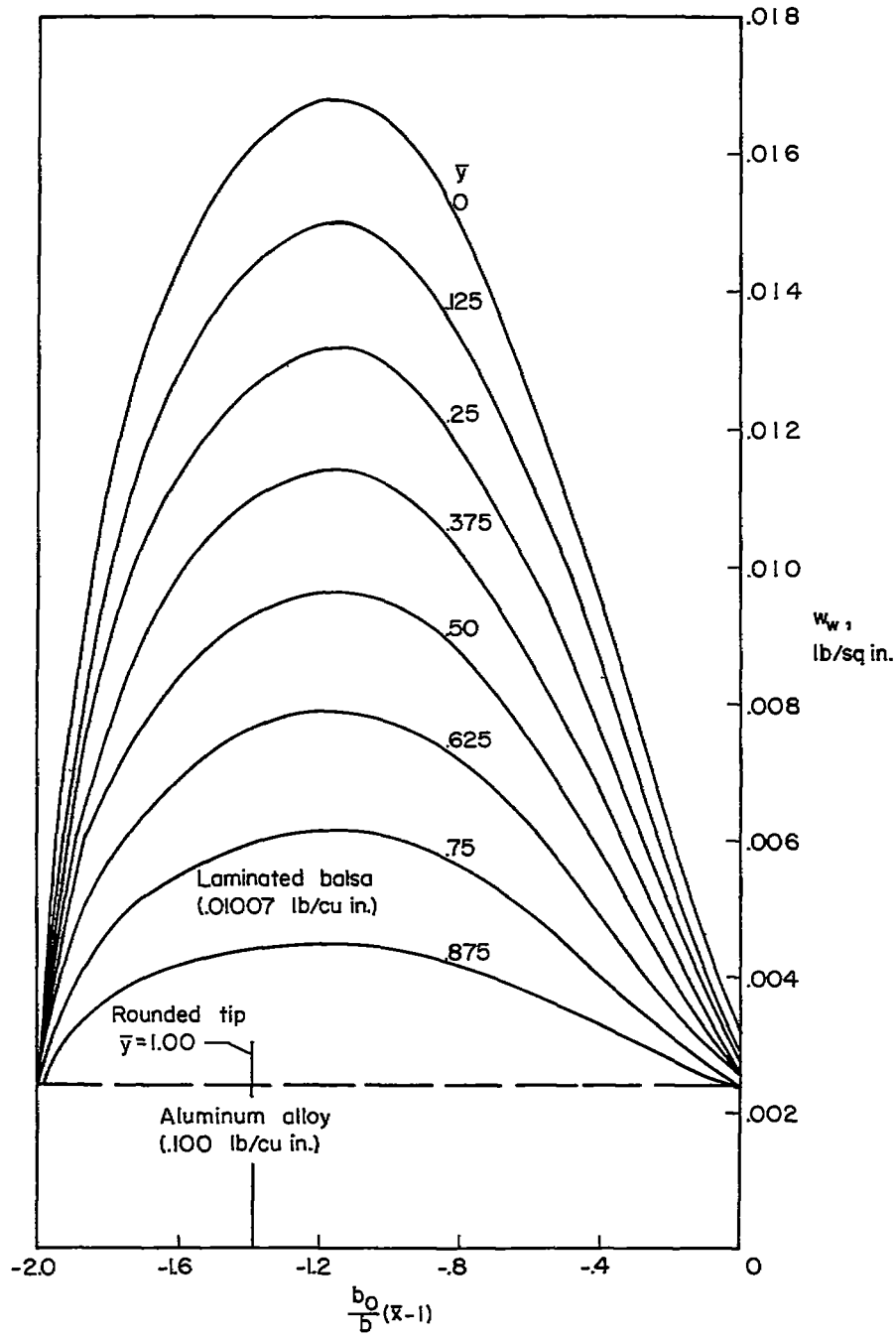


(a) Chordwise distribution.

Figure 3.- Weight distributions of model.

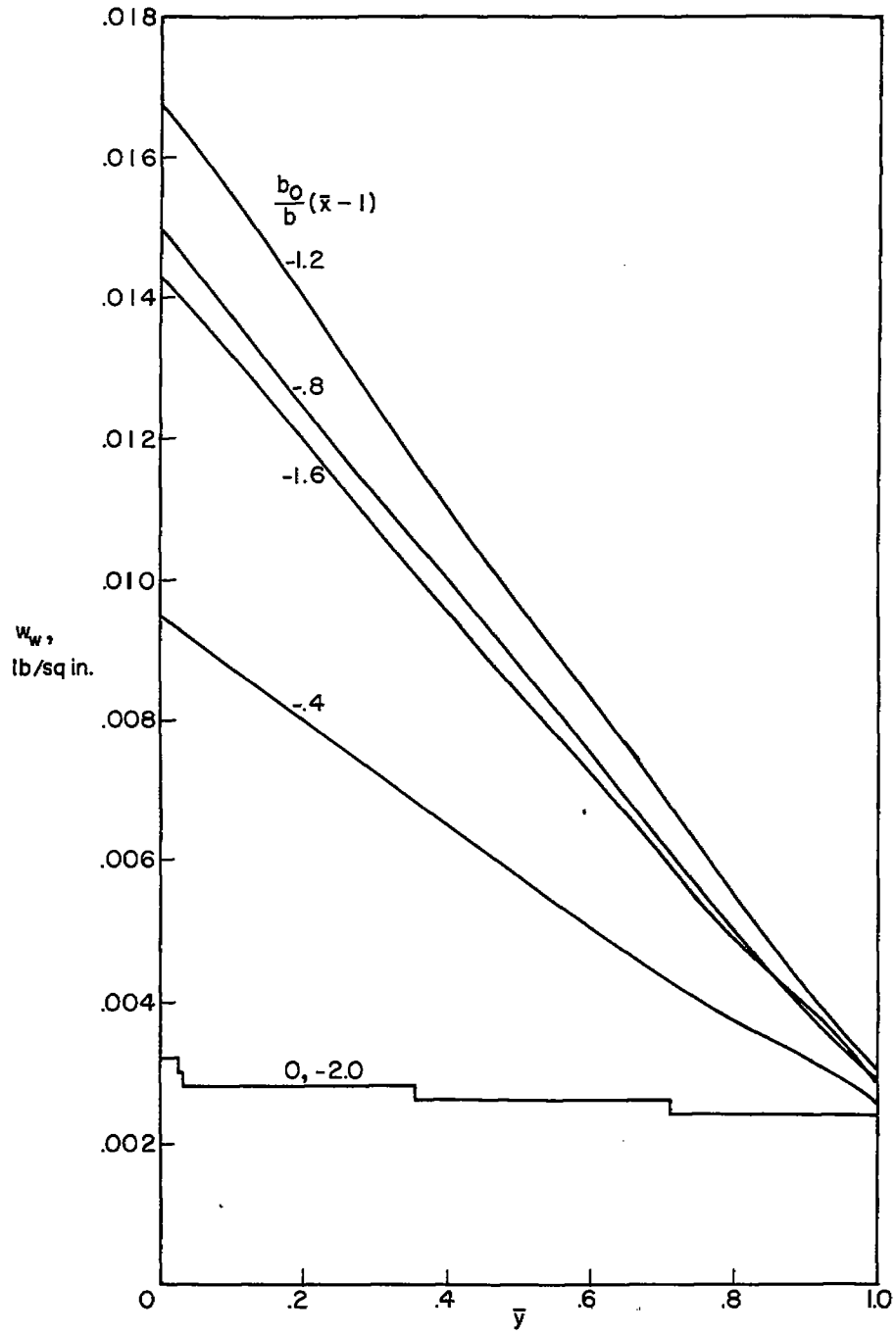


(b) Spanwise distribution.

Figure 3.- Concluded.

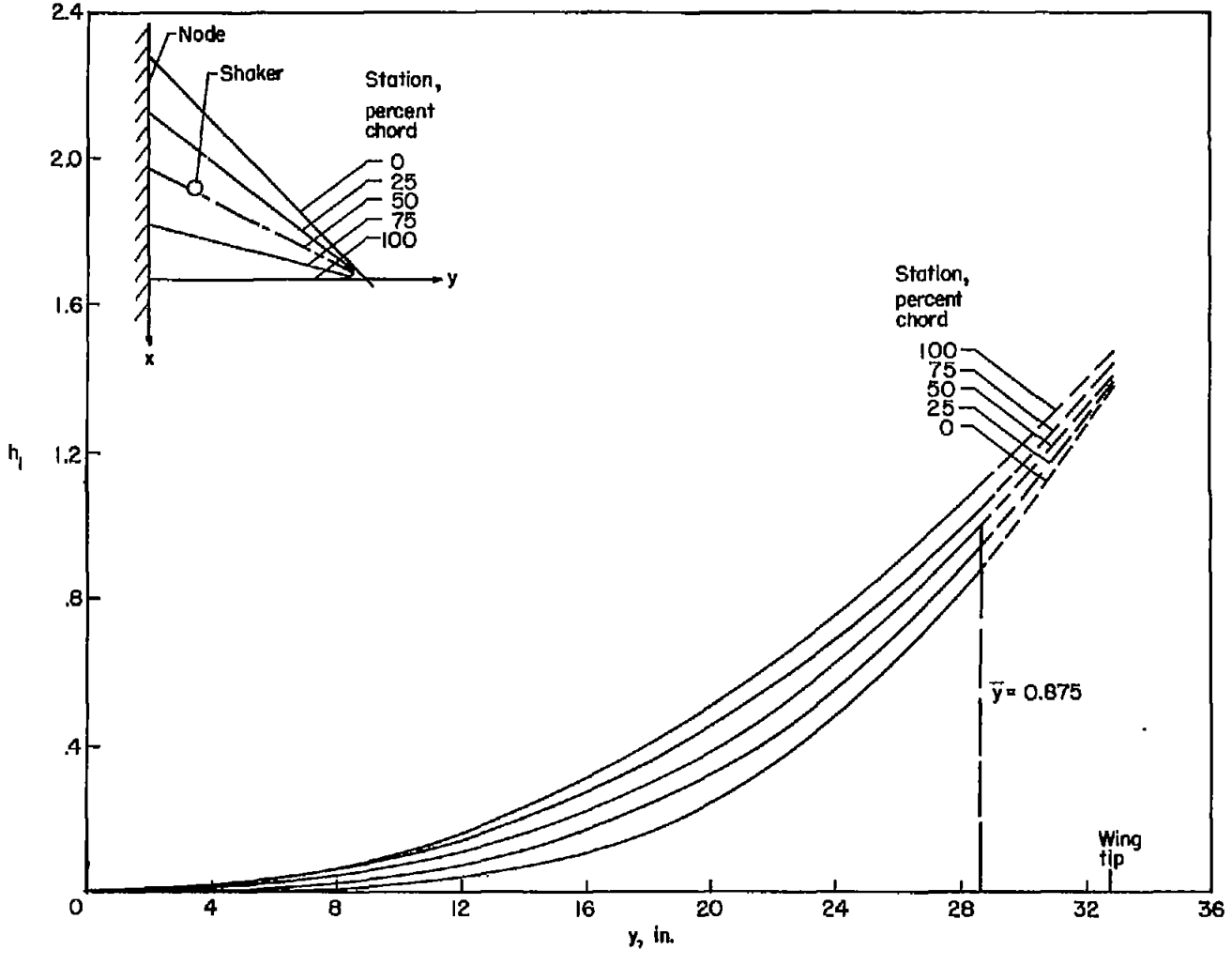


(a) First mode. Frequency, 21 cps.

Figure 4.- Experimental natural modes of vibration. Dashed curves indicate extrapolations.

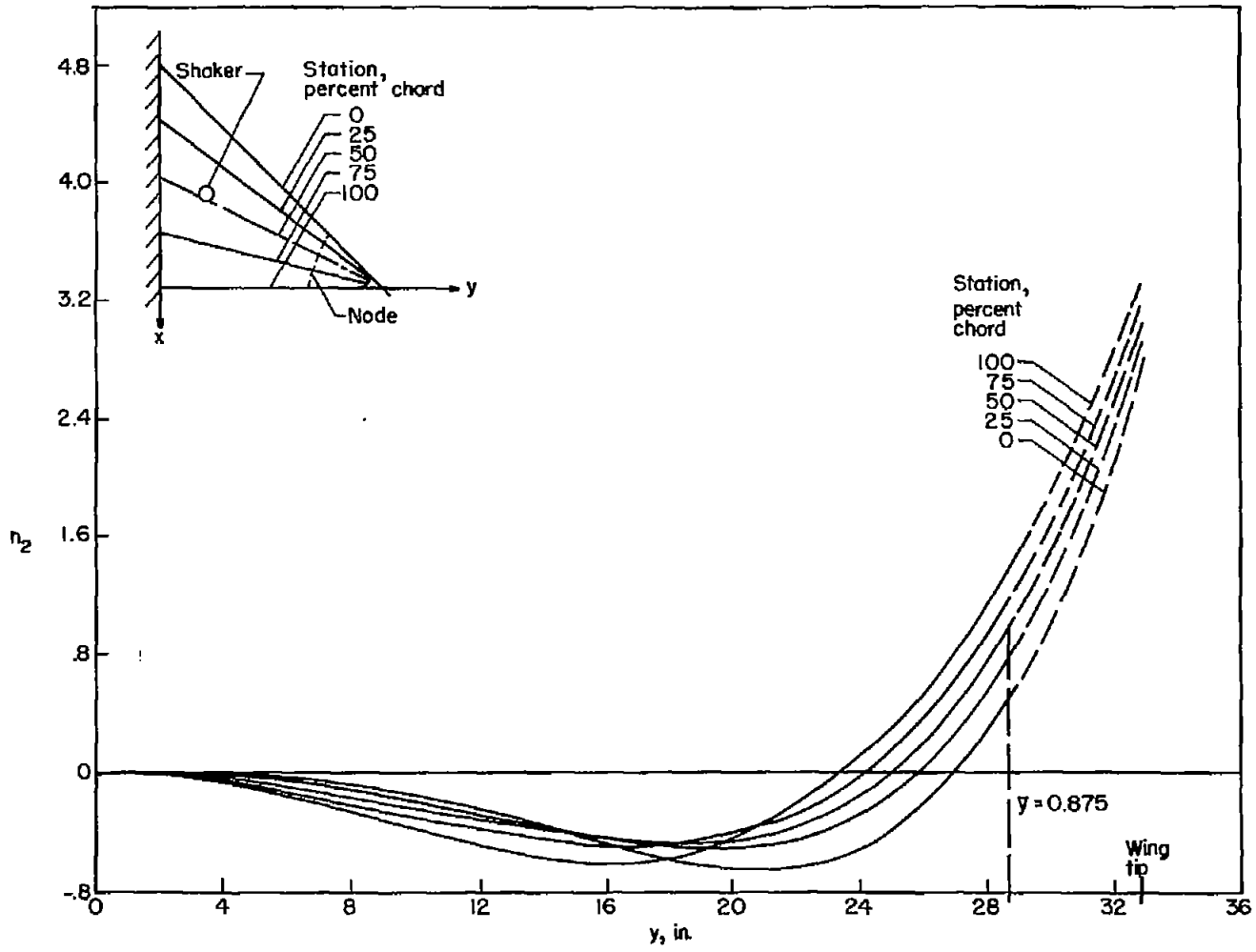


(b) Second mode. Frequency, 52.5 cps.

Figure 4.- Continued.

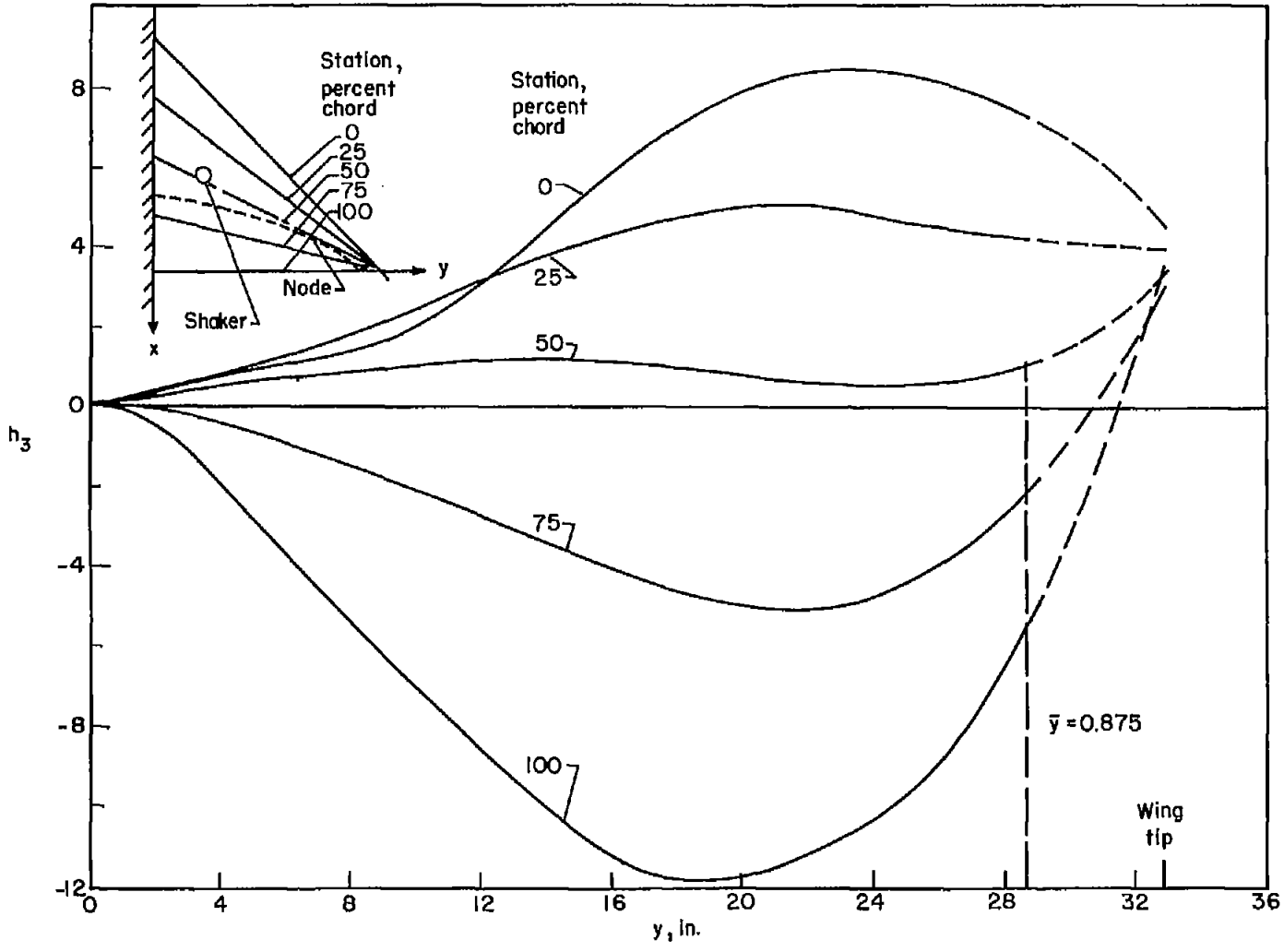


(c) Third mode. Frequency, 77 cps.

Figure 4.- Continued.

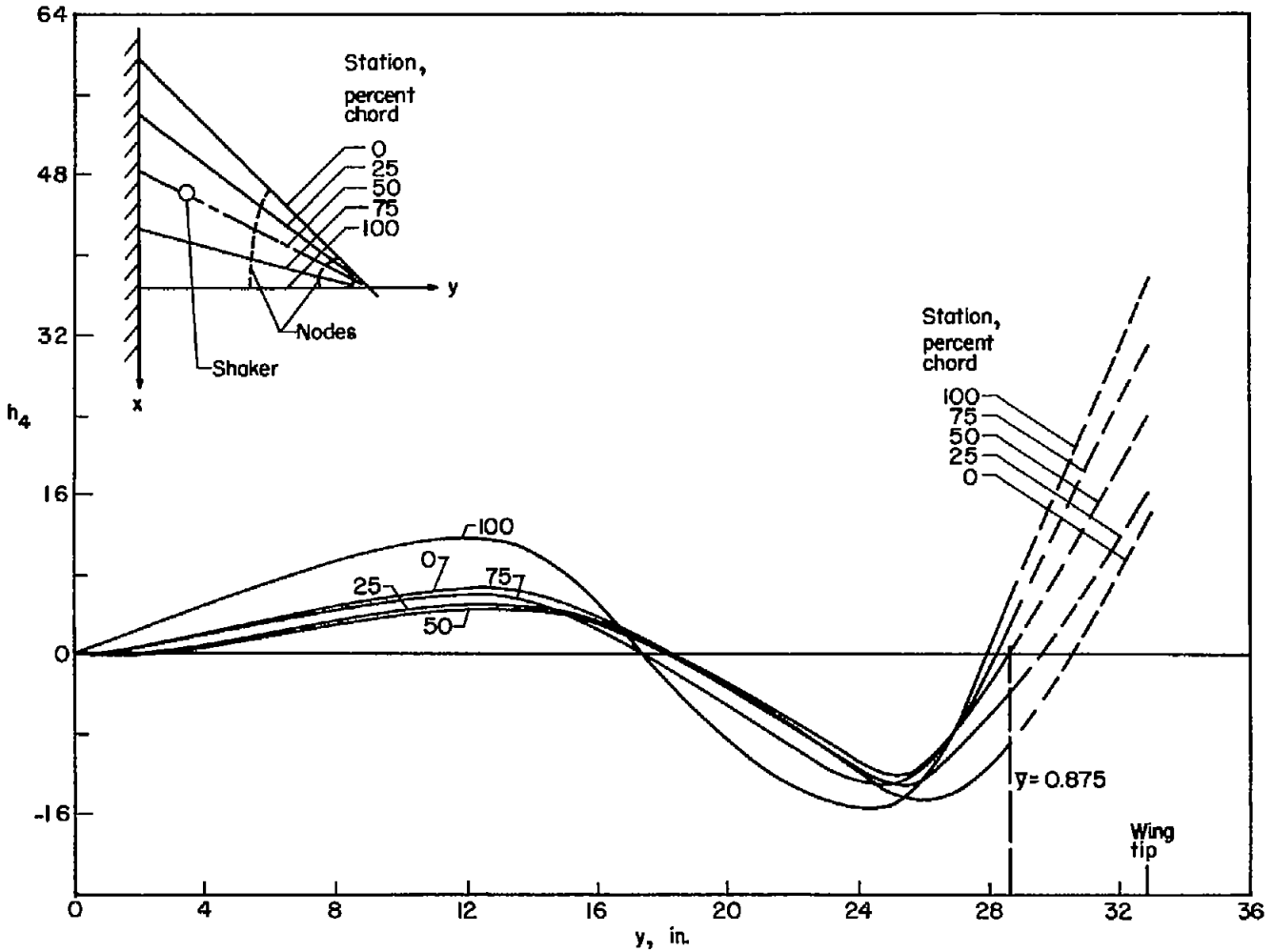


(d) Fourth mode. Frequency, 107 cps.

Figure 4.- Concluded.

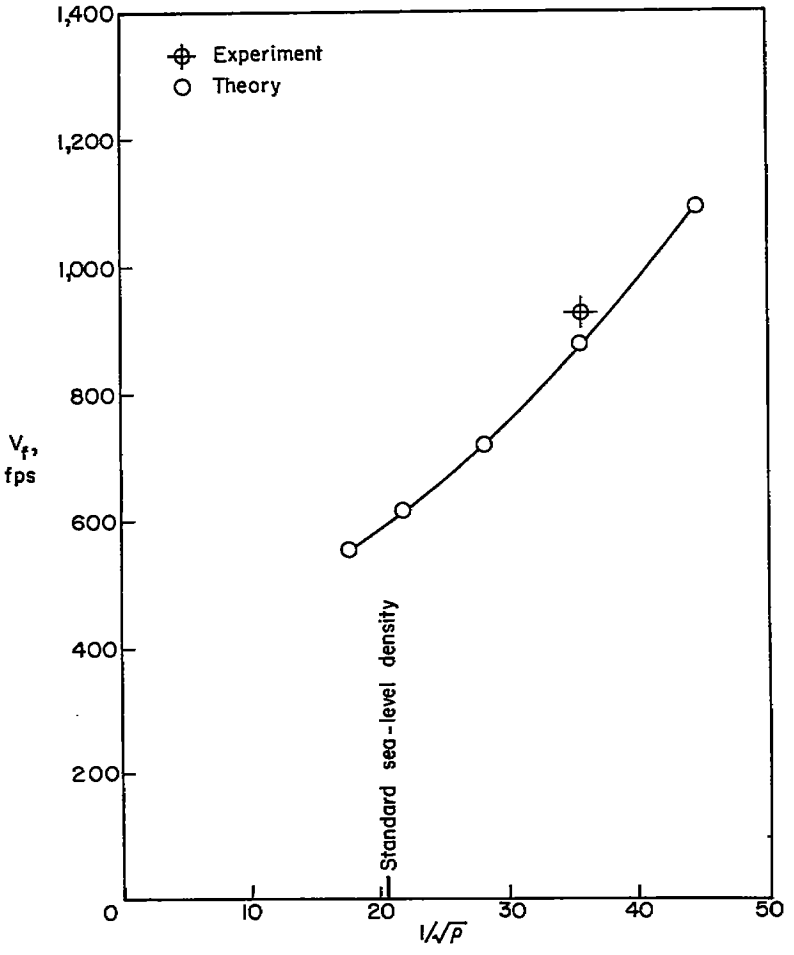


Figure 5.- Effect of density on calculated flutter speed for a Mach number of 0.85.

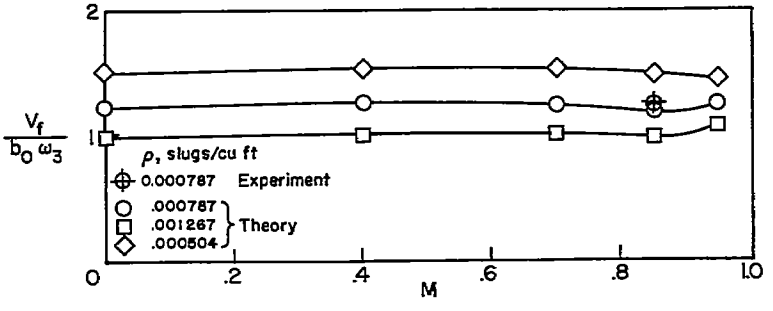


Figure 6.- Effect of Mach number on calculated flutter speed for various densities.

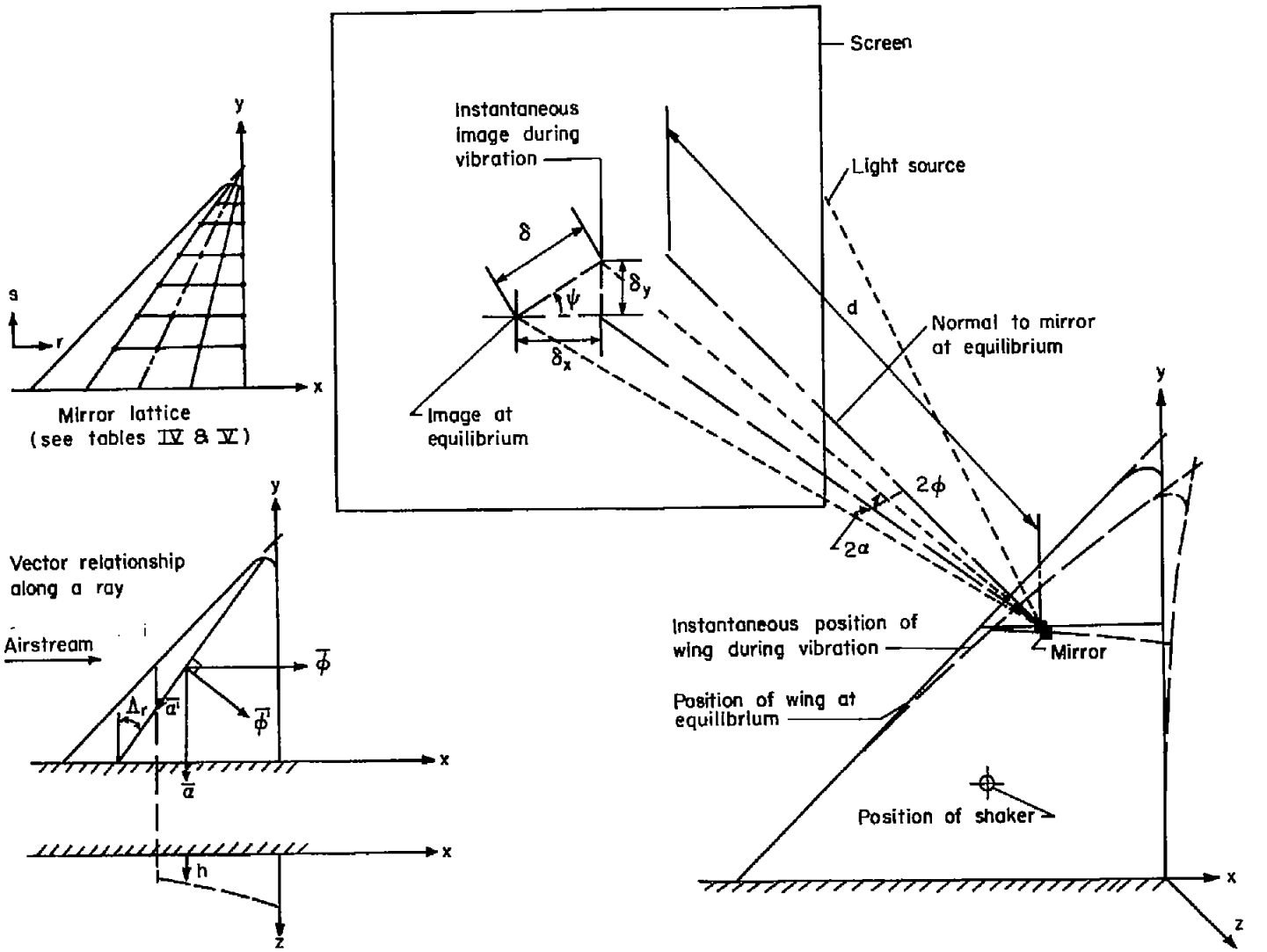


Figure 7.- Schematic diagram of apparatus used to measure natural-vibration-mode shapes. All directions are considered positive as shown; z is considered positive downward.



NACA - Langley Field, Va.